Frontside scattering structures for enhanced performance in flexible ultrathin crystalline silicon solar cells

Baomin Wang,[a] Tongchuan Gao,[b] Ziyu Zhou,[b] Pafchek Bradley,[b] and Paul W. Leu[b,*]

[a]The Pennsylvania State University, Department of Electrical Engineering, University Park, State College, Pennsylvania, United States

[b]University of Pittsburgh, Department of Industrial Engineering, Pittsburgh, Pennsylvania, United States

Abstract. We demonstrate that frontside scattering structures combining a metal nanomesh transparent electrode with dielectric nanosphere (NS) arrays may improve the performance of ultrathin crystalline silicon (c-Si) solar cells. The increased light scattering as characterized by increased haze from these structures leads to longer path lengths within the c-Si and thus, higher short-circuit current densities and improved power conversion efficiencies. We demonstrate a 69% improvement in power conversion efficiency with metal nanomesh/NS coatings compared to indium tin oxide. Furthermore, we demonstrate the ultrathin film c-Si solar cells are robust under repeated bending. [DOI: 10.1117/1.JPE.8.030501]

Keywords: transparent conductor; haze factor; ultrathin silicon; flexible; absorption enhancement.

Paper 18084L received Jun. 7, 2018; accepted for publication Aug. 27, 2018; published online Sep. 14, 2018.

1 Introduction

Ultrathin film crystalline silicon (c-Si) photovoltaics have advantages over conventional bulk c-Si solar cells, such as less material usage and lower cost. Conventional bulk c-Si solar cells are 200 to 300 μm in thickness. Not only do thin films use less material, but they enable the use of poorer quality material with shorter minority carrier diffusion lengths since carriers do not have to diffuse as far to be collected. Ultrathin c-Si may also enable flexible solar cells that are lightweight and bendable and may be incorporated into a variety of unique materials, such as paper, cloth, or plastics. Flexible solar cells are easy to transport and install and may be integrated into crative applications, such as clothing, curtains, paper, and furniture. A large number of efforts have focused on organic[1,2] or amorphous silicon[3,4] solar cells, but the poor minority carrier lifetime and low carrier mobility of these materials have limited their solar conversion efficiency.

One of the main challenges with ultrathin c-Si is that c-Si is not a strong absorber of sunlight in the near-infrared region. Additional structures must be incorporated into the Si to improve its absorption and efficiency. Many nanostructures have been demonstrated for subwavelength light trapping, such as nanowires,[5–10] nanoholes,[8,11] nanocones,[12–14] or photonic crystals.[15–18] Metal nanostructures, such as nanoparticle arrays[19–21] and nanogrooves,[22] have also been studied. However, the additional Si/metal interfaces or Si surfaces from these other approaches result in higher internal quantum efficiency losses from increased surface recombination.

Another approach to light trapping is to increase the scattering of photons into the c-Si, which increases the light's path length inside the c-Si and, hence, increases its absorption.[23,24] Typically, solar cells utilize a quarter-wave thickness antireflection layer coating to reduce reflection losses at interfaces and have a top contact consisting of a metal busbar and fingers or

*Address all correspondence to: Paul W. Leu, E-mail: pleu@pitt.edu

a transparent conductive oxide.[25] However, these structures are thin film layers that do not provide for any light scattering into the underlying active region. Recently, we demonstrated through simulations and experiments that a high index of refraction dielectric nanospheres (NS) on the frontside of c-Si thin film structures can improve power conversion efficiency (PCE) substantially by scattering incident light into the underlying absorber layer.[26,27] We have also recently shown that metal nanomeshes may be engineered for light scattering or haze.[28,29] In this work, we integrate both metal nanomeshes and NS coatings onto a c-Si ultrathin film solar cell and demonstrate improvements in efficiency as well as flexiblity. The PCE of c-Si solar cell with metal nanomesh is improved by 53% compared to that of c-Si solar cell with indium tin oxide (ITO). More importantly, the metal nanomesh has superior flexibility to ITO, which significantly enhances the flexibility and durability of the c-Si thin film solar cells. With the introduction of a dielectric NS monolayer array on top of the metal nanomesh, the scattering of light is further enhanced, and as a result, the PCE of the c-Si solar cell can be increased by an additional 11% or 69% compared to the original ITO.

2 Results and Discussion

Figure 1(a) shows a schematic of our ultrathin film c-Si solar cell structure that consists of a c-Si film between a Ag metal nanomesh front transparent electrode and a Ti/Ag back contact. The c-Si layer is doped n+, p, and p+ from top to bottom. The metal nanomesh is about 35-nm thick with a pitch of 1300 nm and hole diameter 1200 nm, which is fabricated by the microsphere lithography method.[28] The metal nanomesh has a sheet resistance $R_s \approx 10\ \Omega/\text{sq}$ compared to 30 to 40 Ω/sq for ITO with a thickness about 100 nm, which is the optimal thickness for J_{SC} based on our measurements. On top of the metal nanomesh sits a closely packed hexagonal lattice monolayer of 800-nm-diameter polystyrene (PS) NSs with a refractive index of about 1.59, which were coated on top of the c-Si thin film solar cell. Figure 1(b) shows a scanning electron microscope (SEM) image of the top view of the PS NS hexagonal array. The NS layer is closely packed and uniform over the solar cell. Figure 1(c) shows a cross-section SEM image of the solar cell. The c-Si film has a thickness of 14.7 μm, which is slightly thinner than that in our previous paper where the c-Si was 15.0-μm thick.[27] Our previous simulation results indicated that the ultimate efficiency is relatively insensitive to PS NS diameters higher than 800 nm.[27] Larger diameter NSs are difficult to coat uniformly on substrates and may also exhibit higher parasitic absorption from impurities.

Figure 2(a) plots the current density versus voltage ($J-V$) curves of the solar cells measured under the illumination of an AM1.5 global solar simulator. The short-circuit current density J_{sc} of the solar cell with ITO as front contact is 16.2 mA/cm^2. After the front contact was changed from ITO to metal nanomesh, J_{sc} increased to 21.2 mA/cm^2. J_{sc} increased further to 23.4 mA/cm^2 after the PS NS coating.

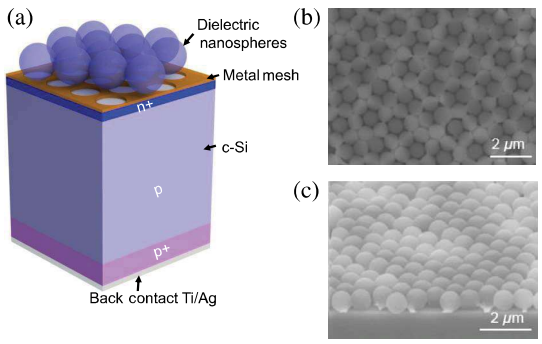

Fig. 1 (a) Schematic of the integrated solar cell with the metal nanomesh and dielectric NSs. The ultrathin film c-Si has a metal nanomesh as the front contact and Ti/Ag as the back contact. A closely packed hexagonal monolayer of 800-nm-diameter PS NSs lies on top of this solar cell. (b) Top view SEM image of the PS NSs on c-Si solar cell. (c) Cross-sectional view of the solar cell with PS NS monolayer on top.

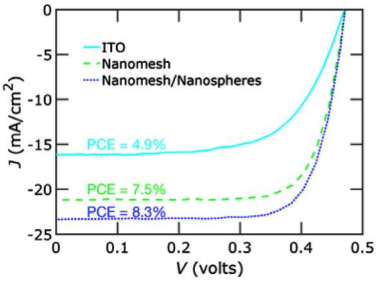

Fig. 2 $J-V$ characteristics of c-Si solar cells with different frontside structures.

Table 1 Photovoltaic properties of the ultrathin c-Si solar cells with different frontside structures.

	J_{sc} (mA/cm^2)	V_{oc} (Volts)	FF (%)	PCE (%)
ITO	16.2	0.47	64	4.9
Nanomesh	21.2	0.47	75	7.5
Nanomesh and NSs	23.4	0.47	75	8.3

Table 1 lists the J_{sc}, open-circuit voltage (V_{oc}), fill factor (FF), and PCE of the three different types of solar cells. As a result of the lower sheet resistance of the metal nanomesh, the FF of the solar cell with metal nanomesh as transparent electrode improved to 75% compared to 64% with ITO as front contact. The PCE of the ultrathin c-Si solar cells improved from 4.9% with ITO to 7.5% with metal nanomesh, which is an improvement of 53%. After the solar cells were coated with PS NSs, the efficiency further improved to 8.3%, which represents an additional 11% improvement or a total improvement over the ITO solar cells of 69%. The V_{oc} of the three cells is all about the same, but the main change is in the J_{sc}, which is indicative of enhanced light trapping without a degradation in surface recombination. Simulation results support our experimental observations. Finite-difference time-domain simulations were used to calculate the maximum short-circuit current density of the ultrathin c-Si solar cells under the assumption that all photons absorbed generate one electron–hole pair and that all carriers are collected without recombination (i.e., at 0 K). The calculated $J_{sc,max}$ for the ultrathin solar cells is 28.5 mA/cm^2 with ITO and 37.9 mA/cm^2 with the metal nanomesh and PS array. The surface passivation and doping profiles may be further optimized to reduce surface recombination at the front and back surfaces. To further understand the results, we characterized both the total transmission and haze of the three different frontside structures. The same structures were fabricated on glass substrates, and then the total transmission and specular transmission were characterized using a spectrophotometer with and without an integrating sphere, respectively. The haze factor is defined as

$$H(\lambda) = \frac{T_{\text{total}}(\lambda) - T_{\text{spec}}(\lambda)}{T_{\text{total}}(\lambda)} \times 100\%, \tag{1}$$

where λ is the free space wavelength, T_{total} is the total transmission, and T_{spec} is the specular transmission. Figure 3 shows the (a) total transmission and (b) haze factor spectra for the three different types of frontside structures.

Table 2 lists the solar transmission, T_{sol}, and solar haze, H_{sol}, for the three different types of frontside structures. The solar integration transmission is calculated from

$$T_{\text{sol}} = \frac{\int b(\lambda) T_{\text{total}}(\lambda) \mathrm{d}\lambda}{\int b(\lambda) \mathrm{d}\lambda}, \tag{2}$$

where $b(\lambda)$ is the photon flux density and $T_{\text{total}}(\lambda)$ is the total optical transmission at wavelength λ. The solar haze is calculated in the same manner.

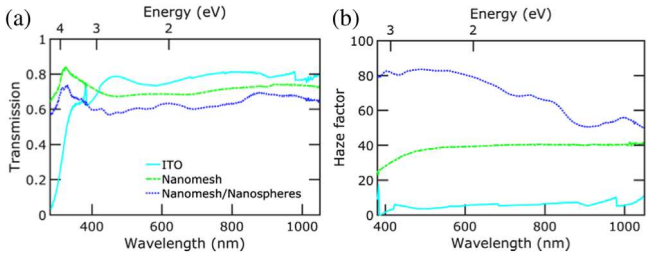

Fig. 3 Measured (a) total transmission and (b) haze of three different frontside structures.

Table 2 The total solar transmission, T_{sol} (%), and solar haze factor, H_{sol} (%), of three different types of contacts.

	T_{sol} (%)	H_{sol} (%)
ITO	77.1	5.7
Nanomesh	70.6	38.5
Nanomesh and NSs	63.0	70.0

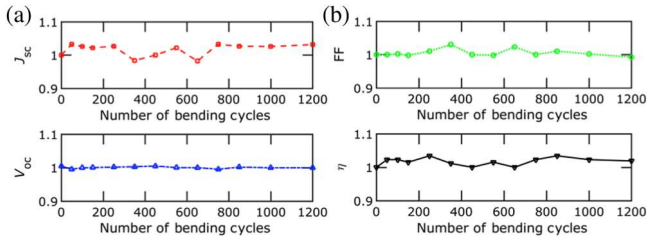

Fig. 4 PCE against the number of bending cycles on a 10-μm c-Si thin film solar cell with metal nanomesh with a geometry of $t = 35$ nm, $a = 1300$ nm, and $w = 100$ nm.

The solar transmission for the ITO is indeed the best, while the metal nanomesh with PS NSs are increasingly worse. However, the ITO has the lowest haze, followed by the metal nanomesh, and then the metal nanomesh with PS NSs. This behavior was similarly found in our evaluation of the performance limits of metal nanomeshes where transmission and haze tend to have a strong negative correlation.[29] We find that the haze factor is much more important in determining the overall performance of the ultrathin c-Si solar cells. While the metal nanomesh with PS NSs has the lowest transparency, the efficiency in ultrathin c-Si solar cells is improved the most with these frontside structures due to increased scattering into the underlying c-Si.

Finally, we assessed the flexible of the solar cell. A 10-μm-thick c-Si solar cell with the Ag metal nanomesh with a thickness of 35 nm, pitch of 1300 nm, and hole diameter of 1200 nm was fabricated and bent around a steel rod with 1-cm diameter. As shown in Fig. 4, the short-circuit density, V_{oc}, FF, and PCE do not change significantly after 1200 cycles of bending. In contrast, ITO is known to form cracks after bending, and the resistivity of ITO has been shown to increase by up to 30 times after 25 cycles of bending.[30]

3 Methods

The ultrathin c-Si film was fabricated from double-side polished p-type (100) c-Si wafers (100-mm diameter, 10 to 20 Ω cm, 475- to 525-μm thickness). The wafer was immersed in 25% KOH solution at 90°C for about 2.5 h to obtain about 14.7-μm-thick c-Si films.[31] The top side of the free standing ultrathin c-Si film was doped n+ via phosphorus spin-on dopant (SOD) (P8545, Honeywell Accuspin), and the back side of the c-Si film was doped

p+ via boron SOD (B40, Honeywell Accuspin). The dopants were diffused into the ultrathin c-Si film by rapid thermal annealing at 900°C for 15 min. After doping, the dopant residue was removed by buffered oxide enchant solution, and then the sample was washed with deionized water thoroughly.

4 Conclusions

In conclusion, we have studied several frontside structures for increased scattering and PCE in ultrathin c-Si solar cells. We find that metal nanomesh contacts with NS coatings enhance the short-circuit current of the solar cells due to increase scattering into the underlying c-Si as characterized by the increased haze factor. We have demonstrated an efficiency enhancement of 69% compared to ITO structures as well as no degradation in performance after bending tests over 1200 cycles. Frontside scattering structures have the potential to significantly improve the performance of solar cells with poor absorption, such as ultrathin c-Si or organic solar cells.

Acknowledgments

This work was supported by the National Science Foundation under Grant No. 1552712.

References

1. M. Kaltenbrunner et al., "Ultrathin and lightweight organic solar cells with high flexibility," *Nat. Commun.* **3**, 770 (2012).
2. C. Lungenschmied et al., "Flexible, long-lived, large-area, organic solar cells," *Sol. Energy Mater. Sol. Cells* **91**(5), 379–384 (2007).
3. T. Soderstrom et al., "Optimization of amorphous silicon thin film solar cells for flexible photovoltaics," *J. Appl. Phys.* **103**, 114509 (2008).
4. Y. Ichikawa et al., "Production technology for amorphous silicon-based flexible solar cells," *Sol. Energy Mater. Sol. Cells* **66**(1), 107–115 (2001).
5. V. Sivakov et al., "Silicon nanowire-based solar cells on glass: synthesis, optical properties, and cell parameters," *Nano Lett.* **9**, 1549–1554 (2009).
6. L. Tsakalakos et al., "Silicon nanowire solar cells," *Appl. Phys. Lett.* **91**, 233117 (2007).
7. D. R. Abujetas, R. Paniagua-Domnguez, and J. A. Snchez-Gil, "Unraveling the Janus role of Mie resonances and leaky/guided modes in semiconductor nanowire absorption for enhanced light harvesting," *ACS Photonics* **2**, 921–929 (2015).
8. S. Aixue et al., "Nanowire and nanohole silicon solar cells: a thorough optoelectronic evaluation," *Prog. Photovoltaics* **23**, 1734–1741 (2015).
9. B. Hua et al., "Rational geometrical design of multi-diameter nanopillars for efficient light harvesting," *Nano Energy* **2**(5), 951–957 (2013).
10. M. I. Kayes and P. W. Leu, "Comparative study of absorption in tilted silicon nanowire arrays for photovoltaics," *Nanoscale Res. Lett.* **9**(1), 620 (2014).
11. K.-Q. Peng et al., "High-performance silicon nanohole solar cells," *J. Am. Chem. Soc.* **132**, 6872–6873 (2010).
12. Z. Y. Wang et al., "Broadband optical absorption by tunable Mie resonances in silicon nanocone arrays," *Sci. Rep.* **5**, 7810 (2015).
13. B. Wang and P. W. Leu, "Enhanced absorption in silicon nanocone arrays for photovoltaics," *Nanotechnology* **23**(19), 194003 (2012).
14. C.-M. Hsu et al., "Wafer-scale silicon nanopillars and nanocones by Langmuir–Blodgett assembly and etching," *Appl. Phys. Lett.* **93**, 133109 (2008).
15. B. Wang, K. P. Chen, and P. W. Leu, "Engineering inverse woodpile and woodpile photonic crystal solar cells for light trapping," *Nanotechnology* **27**(22), 225404 (2016).
16. H. Sai et al., "High-efficiency microcrystalline silicon solar cells on honeycomb textured substrates grown with high-rate VHF plasma-enhanced chemical vapor deposition," *Jpn. J. Appl. Phys.* **54**(8S1), 08KB05 (2015).

17. R. Biswas et al., "Enhanced nanocrystalline silicon solar cell with a photonic crystal back-reflector," *Sol. Energy Mater. Sol. Cells* **94**(12), 2337–2342 (2010).
18. M. D. Zoysa et al., "Enhanced efficiency of ultrathin (500 nm)-film microcrystalline silicon photonic crystal solar cells," *Appl. Phys. Express* **10**(1), 012302 (2017).
19. B. Ding et al., "Synergistic effect of surface plasmonic particles in PbS/TiO_2 heterojunction solar cells," *Sol. Energy Mater. Sol. Cells* **128**, 386–393 (2014).
20. T. Gao et al., "Designing metal hemispheres on silicon ultrathin film solar cells for plasmonic light trapping," *Opt. Lett.* **39**, 4647–4650 (2014).
21. L.-B. Luo et al., "Surface plasmon resonance enhanced highly efficient planar silicon solar cell," *Nano Energy* **9**, 112–120 (2014).
22. V. E. Ferry et al., "Plasmonic nanostructure design for efficient light coupling into solar cells," *Nano Lett.* **8**(12), 4391–4397 (2008).
23. G. Han et al., "Towards high efficiency thin film solar cells," *Progr. Mater. Sci.* **87**, 246–291 (2017).
24. A. Zitzler-Kunkel et al., "NIR-absorbing merocyanine dyes for BHJ solar cells," *Chem. Mater.* **26**(16), 4856–4866 (2014).
25. R. B. Wehrspohn, U. Rau, and A. Gombert, *Photon Management in Solar Cells*, John Wiley & Sons, Weinheim, Germany (2015).
26. B. Wang and P. W. Leu, "High index of refraction nanosphere coatings for light trapping in crystalline silicon thin film solar cells," *Nano Energy* **13**, 226–232 (2015).
27. B. Wang, T. Gao, and P. W. Leu, "Broadband light absorption enhancement in ultrathin film crystalline silicon solar cells with high index of refraction nanosphere arrays," *Nano Energy* **19**, 471–475 (2016).
28. T. Gao et al., "Uniform and ordered copper nanomeshes by microsphere lithography for transparent electrodes," *Nano Lett.* **14**(4), 2105–2110 (2014).
29. G. Tongchuan et al., "Fundamental performance limits and haze evaluation of metal nanomesh transparent conductors," *Adv. Opt. Mater.* **6**(9), 1700829 (2018).
30. X. He et al., "A highly conductive, flexible, transparent composite electrode based on the lamination of silver nanowires and polyvinyl alcohol," *J. Mater. Chem. C* **2**, 9737–9745 (2014).
31. C. Wang et al., "Carbon nanotube electronics—moving forward," *Chem. Soc. Rev.* **42**, 2592–2609 (2013).